

# Analysis of Transonic Flow on a Slender Delta Wing Using CFD

L. A. Schiavetta\*

*University of Glasgow, Glasgow, G12 8QQ, UK*

O. J. Boelens<sup>†</sup>

*National Aerospace Laboratory NLR, Amsterdam, The Netherlands*

W. Fritz<sup>‡</sup>

*EADS Military Air Systems, Munich, Germany*

The behaviour of the flow over slender delta wings under transonic conditions is highly complex. With the occurrence of a number of shocks in the flow the behaviour of vortex breakdown is quite different to that for subsonic flow. This investigation considers this behaviour over the  $65^\circ$  sharp leading edge delta wing used in the 2nd International Vortex Flow Experiment (VFE-2) using Computational Fluid Dynamics. Three institutions involved in the VFE-2 have collaborated to consider the wing under conditions of  $M = 0.85$  and  $Re = 6 \times 10^6$  at two incidences:  $\alpha = 18.5^\circ$  and  $23^\circ$ . The flow solutions are compared to existing experimental data and show good agreement for the cases considered. However, a discrepancy with the experimental data is shown where the critical incidence for the onset of vortex breakdown on the wing is under-predicted. From analysis of the solutions, it is determined that the onset of vortex breakdown is highly dependent on the vortex strength and the strength and location of the shocks in the flow. The occurrence of a critical relationship between these parameters is suggested for vortex breakdown to occur and is used to explain the discrepancies between the computational and experimental results based on the under-prediction of the vortex core axial velocity. A sensitivity study of the flow to a number of computational factors, such as turbulence model, is also undertaken. However, it is found that these parameters have little effect on the overall behaviour of the transonic flow.

## Nomenclature

$\alpha$	Angle of incidence
$\alpha_{cr}$	Critical incidence for vortex breakdown
$\Omega$	Rotation Rate
$M_\infty$	Free-stream Mach number
$P_1, P_2$	Pressures defined upstream and downstream of shock surface
$r_c$	Radius of vortex core at point of max. swirl velocity
$Re$	Reynolds number
$Ro$	Rossby number
$U_\theta$	Tangential or Swirl Velocity
$U_x$	Axial Velocity
$x/c_r$	Non-dimensional stream-wise location
$y/s$	Non-dimensional span-wise location

---

\*PhD Candidate, CFD Research Laboratory, Department of Aerospace Engineering, lschiavetta@aero.gla.ac.uk

<sup>†</sup>R & D Engineer, Applied Computational Fluid Dynamics, Department of Flight Physics and Loads, Aerospace Vehicles Division.

<sup>‡</sup>R & D Engineer, Numerical Simulation, Department of Flight Physics.

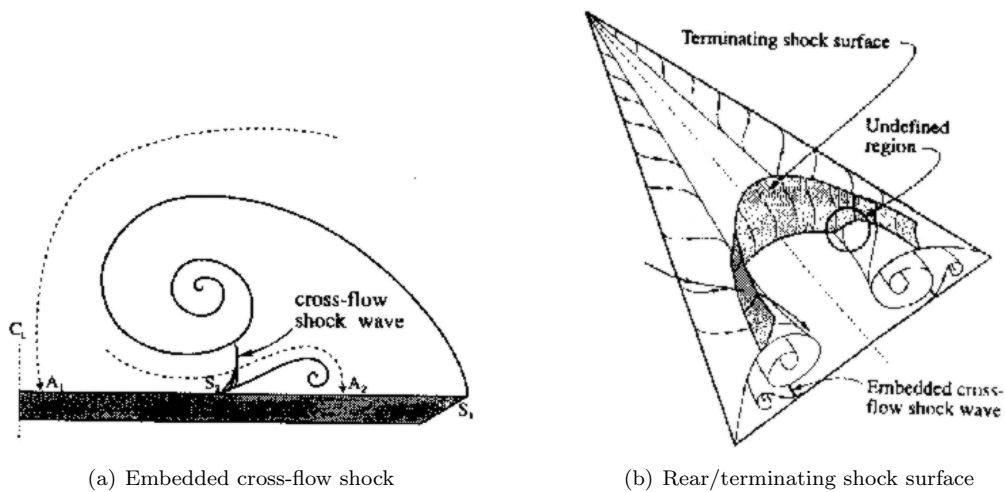


Figure 1. Schematic diagrams showing proposed positions and shapes of shock systems over transonic delta wings (From Ref. 1)

## I. Introduction

MUCH is known about vortical flow over slender, sharp edged delta wings and there have been many reviews which have detailed the vast volume of data available on the subject, both experimental and computational.<sup>2-6</sup> For the most part, this data concerns the subsonic behaviour of the flow and vortex breakdown and thus, it may be said, that generally the flow in this regime is fairly well understood. However, an area of delta wing vortical flow which is not so well understood is the behaviour of the flow under transonic conditions. Within this regime, complex interactions between shockwaves and the leading edge vortex system occur at moderate to high incidences. For this reason, transonic vortical flow and vortex breakdown is one aspect of the second “International Vortex Flow Experiment” (VFE-2), which is taking place as part of the NATO RTO AVT-113 Task Group, currently underway. The work of the VFE-2 continues on from the first International Vortex Flow Experiment (VFE-1)<sup>7</sup> carried out in the late eighties, which was used to validate the inviscid CFD codes of the time. Much progress has been made in both experimental and computational aerodynamics, particularly in the application of RANS turbulence models since the conclusion of the VFE-1. Therefore, it was proposed by Hummel<sup>8</sup> that a second experiment should be undertaken to provide a new, comprehensive database of both computational and experimental results for various flow regimes. It is intended that this new database of information would improve computational code validation and development and aid in further understanding of various aspects of vortical flow. These include flow over sharp and rounded leading edged, slender delta wings using both experimental and numerical techniques for a range of incidences, Mach and Reynolds numbers, which includes the transonic regime detailed in this paper.

From the existing literature on transonic vortical flows, it has been noted that the behaviour of the flow is somewhat different to vortical flow in the subsonic regime. With an increase in Mach number, the size and shape of the vortex system changes<sup>9</sup> and the primary vortex is found to sit progressively closer to the wing surface. At transonic Mach numbers, the leading edge vortices take on a relatively flat appearance and despite an increased proximity to the wing, the vortex system creates a much reduced suction peak incident on the wing. Further to these changes in flow structure comes the appearance of shockwaves in the flow. These shock waves are caused by localised supersonic flow regions and generally appear to maintain flow equilibrium.

A number of investigations, both experimental and numerical have been carried out, both as part of the VFE-1 and since, which have looked at the occurrence and behaviour of shockwaves in vortical flows for varying transonic conditions.<sup>1,10-16</sup> From these investigations, a number of shockwave systems have been observed and detailed in the literature. Elsenaar and Hoeijmakers<sup>10</sup> described two main systems based on conjecture and experimental results. These are located: 1) Underneath the primary vortex, at an approxi-

mately constant spanwise position, outboard of the primary suction peak, and 2) On the aft section of the wing, close to the trailing edge and perpendicular to the plane of symmetry. These are termed cross-flow and rear/terminating shocks, respectively. These two shock systems have also been determined from other experimental results using surface pressure<sup>12</sup> and flow visualisation methods,<sup>1,13</sup> and also from computational results employing inviscid,<sup>11</sup> laminar<sup>14,15</sup> and turbulent<sup>16</sup> methods. From these studies, the shape and general behaviour of these shocks have been detailed and Figure 1 shows schematics of the suggested location of these shocks relative to the leading edge vortices. Other shock systems found occurring in transonic vortical flows include shocks above the leading edge vortices<sup>12,16</sup> and inboard of the primary vortex parallel to the surface.<sup>16</sup> The occurrence of these shocks and other significant flow features on the wing, such as vortex breakdown, were considered for a range of incidences and Mach numbers at a constant Reynolds number by Elsenaar and Hoeijmakers<sup>10</sup> and the resulting boundary plot of these behaviours is shown in Figure 2. From this diagram, it is clear, that for transonic flow both rear and cross-flow shocks appear for increasingly lower incidences. The fact that the incidence at which vortex breakdown occurs decreases with increasing Mach number is also shown.

The occurrence of these shockwave systems in the flow introduces the complex behaviour of shock/vortex interactions. These interactions have a significant effect on vortex breakdown and the breakdown behaviour is quite different to that witnessed for subsonic vortical flows where the onset of breakdown is relatively gradual with increasing incidence.<sup>17</sup> Vortex breakdown under transonic conditions is quite abrupt with the location of breakdown shifting upstream by as much as 30% chord in a single  $1^\circ$  interval.<sup>10,11</sup> An interaction between the rear/terminating shock and the primary vortex has been found, in some cases, to cause breakdown<sup>1,14</sup> and with increasing incidence this shock can jump upstream quite abruptly. The upstream shift of the shock is likely to be caused by the need to restore flow equilibrium in reaction to changes in the flow behaviour<sup>1</sup> caused by an increase in incidence. If the conditions are sufficient that the shock/vortex interaction causes breakdown, the sudden upstream movement of the shock will also cause the breakdown location to move upstream. In the investigation by Elsenaar and Hoeijmakers<sup>10</sup> it was found that after this upstream shift has occurred, a second rear shock is found to appear in its place close to the trailing edge. At moderate incidences, the location of the shock moves downstream toward the trailing edge with an increase in Mach number,<sup>10</sup> suggesting that its strength increases, this also appears to be true for increasing incidence. This is clearly shown in Figure 3, which shows the behaviour of the flow at the symmetry plane for both pre- and post-breakdown cases. Coincident with the onset of transonic breakdown is a sudden and complete loss of suction on the wing characterised by the collapse of the surface pressure distribution suction peak.<sup>18</sup> Subsequent pressure distributions downstream of breakdown have been found to be quite flat. This has obvious detrimental effects on the aerodynamic performance of the wing planform, particularly when coupled to the abrupt nature of the breakdown. Aerodynamic characteristics such as lift coefficient distribution, stall and pitch may all be badly affected by such flow behaviour.

From the literature it has also been noted that it is possible for a terminating shock system to exist without the breakdown of the vortical system<sup>1</sup> particularly at lower incidences. In Figure 1, it is shown that for an incidence of approximately  $15^\circ$ , the rear/terminating shock curves downstream and appears to intersect the vortex core. However, breakdown does not occur for this case and it was suggested that the shock instead sits above the vortex core and no interaction occurs. What happens at this point is not well understood, and whether interaction occurs for lower incidences is not known conclusively. From the study of the interaction between longitudinal vortices and normal shocks in supersonic flow<sup>19</sup> it has been

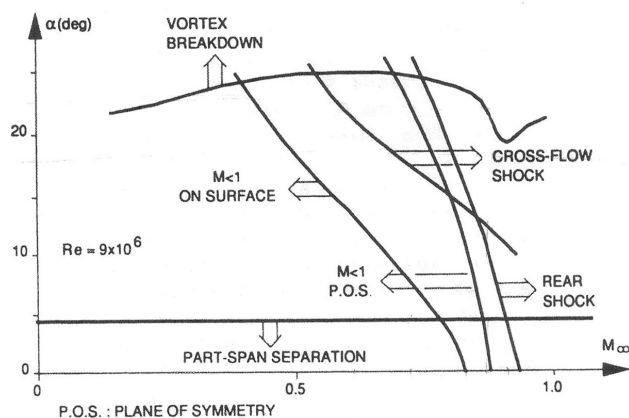


Figure 2. A summary of the flow features for various Mach numbers and incidences (From Ref. 10)

found that it is possible for a vortex to pass through a normal shock without being weakened sufficiently to cause breakdown. However, the flow over slender delta wings is more complex as the shock does not appear to be normal to the freestream in the vortex core region.<sup>1</sup> Therefore, further investigation is needed to consider the behaviour and onset of vortex breakdown, particularly with respect to shock/vortex interactions.

To consider this type of behaviour, three institutions involved in the VFE-2; EADS-MAS, the University of Glasgow and NLR have undertaken a number of computational calculations on a sharp leading edge  $65^\circ$  delta wing under transonic flow conditions. All calculations were performed at a Mach number of  $M = 0.85$  and Reynolds number of  $Re = 6 \times 10^6$  and for two incidences:  $18.5^\circ$  and  $23^\circ$ . From the diagram in Figure 2 it is clear that both these cases fall within the regions where it is highly likely that both cross-flow and rear shocks will occur in the flow. Thus, the occurrence of these shocks will be analysed for the flow solutions. Comparisons between each of the calculations and with available experimental data will be made and consideration of the sensitivity of the flow behaviour to a number of computational factors will be detailed. Further to these comparisons, the nature and behaviour of transonic vortex breakdown will be considered with respect to the discussion given above.

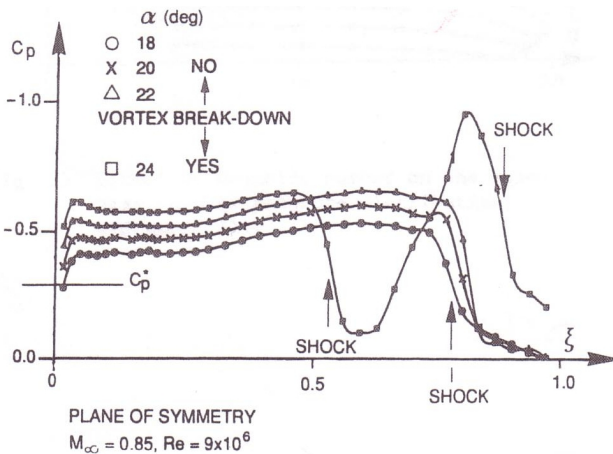


Figure 3. Chordwise pressure coefficient distribution at the symmetry plane for a range of incidences pre- and post-breakdown (From Ref. 10)

## II. Investigation Set up

The geometry chosen for use in the VFE-2 and, thus, for this investigation, is from the experiments carried out by Chu and Luckring<sup>20-23</sup> in the National Transonic Facility (NTF) at NASA Langley. These experiments considered a  $65^\circ$  delta wing with four leading edge profiles (one sharp and three rounded with small, medium and large radii) for a wide range of conditions both subsonic and transonic and for both test and flight Reynolds numbers. This data has been compiled into a comprehensive experimental database and forms the basis for the investigations of the VFE-2. The geometry is analytically defined for all leading edge profiles, which allows improved correlation between experimental and computational results by reducing geometrical discrepancies. For this investigation, only the sharp leading edge profile is considered. Figure 4 shows the wing situated in the NTF wind tunnel and a brief overview of the analytical dimensions of the wing.

Table 1. Grids and turbulence models used in investigation

Institution	Topology	Size $\times 10^6$	No. of Grid Points on Wing			Turbulence Model
			Spanwise	Streamwise	Normal	
EADS	C-O	$\sim 10.6$	129	257	129	Wilcox $k-\omega$ and Reynolds Stress Model
Glasgow	H-H with O-grid	$\sim 7$	170	228	81	Wilcox $k-\omega$ with $P_\omega$ Enhancer
NLR	C-O	$\sim 4$	192	112	96	TNT $k-\omega$ with $P_\omega$ Enhancer

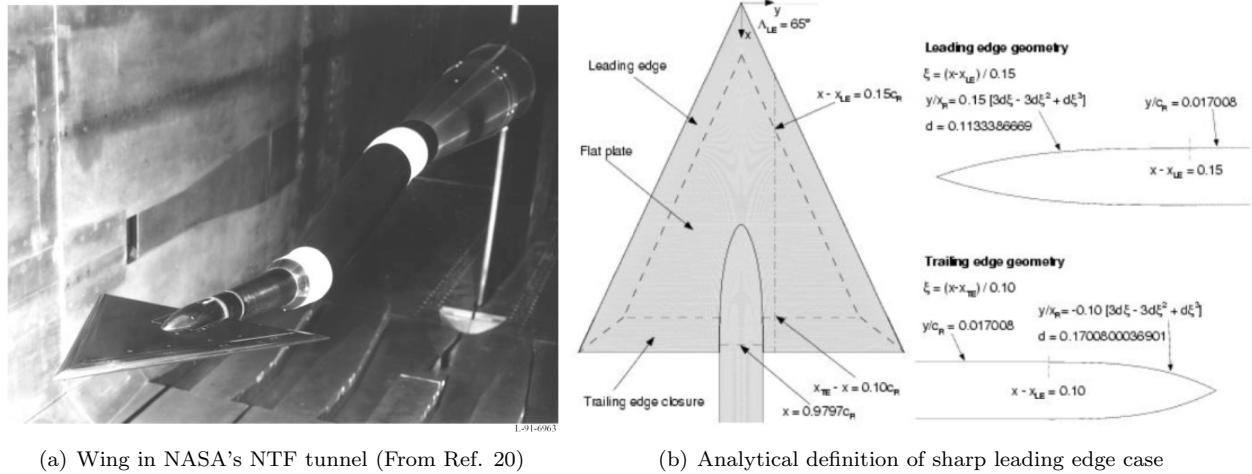


Figure 4. Wing geometry used in investigation

As mentioned above, this work covers the results of three separate institutions, who are collaborating as part of the VFE-2. These are EADS-MAS, the University of Glasgow and NLR using the well-validated 3D Reynolds-averaged Navier-Stokes (RANS) codes; FLOWer 116.17, PMB and ENSOLV respectively. All of these codes have been used and compared in previous work<sup>24</sup> and run using structured, multi-block grids. The solutions from each of the institutions will be compared and verified against each other as well as validated against available experimental data. Detailed descriptions of each of the flow solvers, computational set-up and grids used in the investigation are given in the Appendix and summarised in Table 1.

As detailed in the introduction, it is expected that a number of shock systems will exist in the flow for these conditions. In order to facilitate the identification of these shocks, a shock detection algorithm was used from the CFD Analyzer add-on of the Tecplot post-processing package. The algorithm is based on the work of Lovely and Haines<sup>25</sup> and calculates the locations of shocks based on the criteria of local Mach number and pressure gradients. The algorithm calculates the pressure gradients in the flow and determines possible shock surfaces (pressure gradient is always normal to a shock surface) and then calculates the local Mach vector at each point normal to this surface. At each point in the flow a shock test value is created by using the dot product of the pressure gradient and local Mach vector. Where this test value is greater than one it is proposed that a shock occurs. Due to the negligible thickness of shockwaves occurring in the flow, the algorithm calculates shock surfaces which surround the region where a shock is calculated to form. To allow validation of this algorithm and confirm the locations of the shocks in the flow, the solutions were also analysed using the variables: Mach number, Entropy and pressure gradients (both magnitude and in all directions), which were compared to the shock feature contours produced by the algorithm described above. Thus, considering the distributions of all of these variables and reasoning based on previous investigations, the locations of shocks in the flow were able to be established.

### III. Results

All three sets of calculations were run under the conditions detailed in the preceding sections, and the resulting flow solutions were considered and compared. To allow validation of the computational results, comparisons were made with the experimental pressure coefficient distributions at five streamwise locations on the wing surface,  $x/c_r = 0.2, 0.4, 0.6, 0.8$  and  $0.95$ . The results of these validation comparisons is shown in Figure 5 for both incidences, with the computational results being compared to the corresponding experimental data points. Surface pressure coefficient distributions for each set of results are also shown in Figure 6 with the pre-breakdown case on the left and the post-breakdown case on the right.

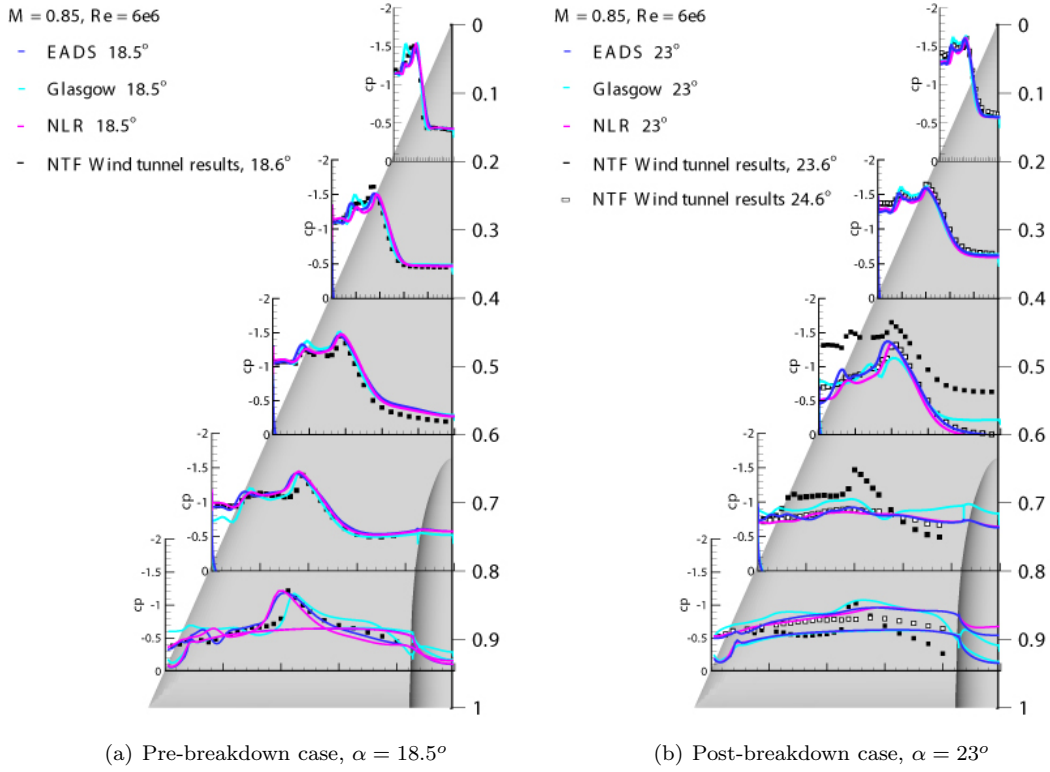


Figure 5. Comparisons between Computational Results and Experiment for all codes for  $M = 0.85$ ,  $Re = 6 \times 10^6$

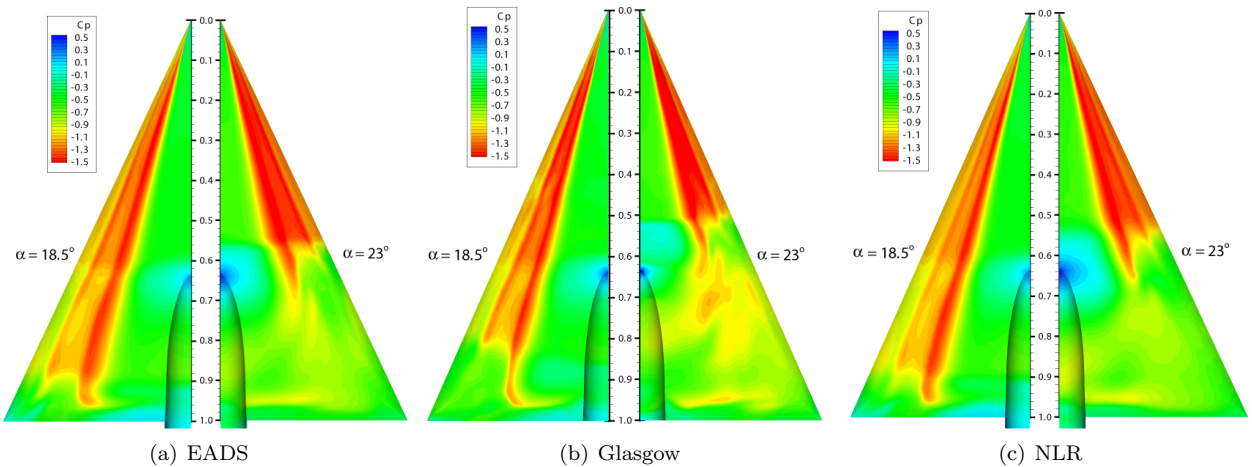


Figure 6. Surface Pressure Coefficient Contours for all results,  $M = 0.85$ ,  $Re = 6 \times 10^6$

### A. $M = 0.85$ , $\alpha = 18.5^\circ$

Referring to the pre-breakdown case first in Figure 5(a), it is clear that the agreement between the computational results and the experimental data is good. For most streamwise locations, the magnitudes and positions of the suction peaks are well predicted. However, the secondary vortex is slightly over-predicted in the Glasgow solution and under-predicted in the EADS and NLR solutions. These discrepancies may be attributed to differences in transition treatment, with both EADS and NLR running fully turbulent calculations and Glasgow setting a forced transition from laminar to turbulent flow at  $x = 0.4$ . A short transition location study was performed by Glasgow, however the flow behaviour was not found to change much for

either an upstream or downstream movement of the location. Overall, the differences in the secondary peaks appear to lessen with increased distance from the apex. Downstream close to the trailing edge at  $x/c_r = 0.95$ , the agreement between each of the computational solutions lessens. Both the EADS and NLR solutions predict the suction peak and sudden increase in pressure further outboard than both the experiment and the Glasgow results. With further consideration, it may be possible to attribute this difference to grid refinement and topology in this region as both the EADS and NLR grids use a conical C-O topology and Glasgow uses an H-H grid, which is not conical and, therefore, more refined close to the trailing edge. This behaviour is also clear from the surface pressure coefficient distributions of Figure 6.

These distributions also show the similarities and differences between each of the flow solutions. For each solution the location of the vortical system is the same with a well defined primary and secondary vortex. However, the Glasgow results has a much more narrow suction peak imprint than the other results. Upstream of the sting tip there is a region of increased pressure at approximately  $x/c_r = 0.6$ , which as will be detailed later, is evidence of a shock occurring in the flow at this point. Downstream of  $x/c_r = 0.8$ , it appears for all cases that the secondary vortex disappears and the primary vortex curves inboard toward the sting region at the trailing edge. This is also clear from consideration of the pressure coefficient plots shown in Figure 5(a), which shows a fairly flat distribution outboard of the primary vortex for  $x/c_r = 0.95$ . From consideration of the behaviour of flow variables through the vortex cores it is found that the secondary vortex breaks down as it approaches the trailing edge but the primary vortex does not. This is shown using the Glasgow results in Figure 7 which shows the secondary breakdown occurring at approximately  $x/c_r = 0.85$ , which is slightly further upstream than for the other two cases. It is fairly unusual for the secondary vortex to breakdown upstream of the primary vortex. However, with closer inspection of the wing geometry in this region it may be possible that this phenomenon is due to the intersection between the leading edge and trailing edge curvature. Alternatively, due to the fact that the Glasgow results are further upstream than for the EADS or NLR solutions and that this location coincides with a second normal shock in the flow, it may be that a type of shock/vortex interaction is occurring. However, it appears that the primary vortex is unaffected. Further consideration of this region and analysis of the flow solutions is needed to determine the causes of this behaviour. Although consideration of the occurrence of shocks and their effect on the flow will be discussed in a later section, this region will not be considered in great detail in this investigation.

## B. $M = 0.85$ , $\alpha = 23^\circ$

For the  $23^\circ$  case, it is clear from Figure 5(b) that close to the apex of the wing i.e.  $x/c_r = 0.2$  and  $0.4$ , the agreement between all the computational solutions and the experimental data is good, with the magnitude and location of the primary and secondary peaks being predicted well. As before, for the pre-breakdown case, the secondary vortex is slightly over-predicted in the Glasgow solution and under-predicted in the EADS and NLR solutions. Downstream of the  $x/c_r = 0.4$  location, the CFD solutions no longer agree well with the experimental results for the  $23.6^\circ$  experimental data point. The predicted pressure coefficient distributions show considerably lower suction peaks at  $x/c_r = 0.6$  and for  $x/c_r = 0.8$  and  $0.95$  there are no discernible peaks at all. Despite this large discrepancy with the experimental data, the CFD solutions all agree well with each other. From consideration of the literature and further investigation of the computational flow solutions, which will be discussed in the following sections, it was determined that these large discrepancies were caused by the occurrence of vortex breakdown in the flow. In the experimental investigation of Houtman and Bannink<sup>18</sup> it was noted that the spanwise pressure distribution just downstream of vortex breakdown shows a collapse in the suction peak, then a complete loss of suction over the wing, similar to that found in these results. Further analysis of the experimental data showed that vortex breakdown occurred at an incidence of  $24.6^\circ$ , which is the next test point in the data set. The surface pressure coefficient distributions from this test point are also included in Figure 5(b) and show a much improved agreement with the computational

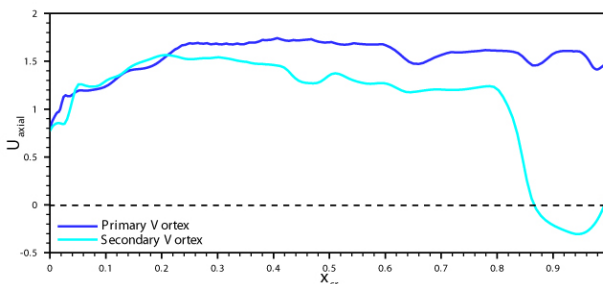


**Figure 7.** Axial velocity through primary and secondary vortex cores,  $\alpha = 18.5^\circ$  (Glasgow Results)

results, confirming that vortex breakdown does indeed appear on the wing for a  $23^\circ$ . Therefore, it may be suggested that although the agreement between the experiment and computations are relatively poor at  $23^\circ$ , this is due to comparing pre- and post-breakdown flows and not to poor computational results. Further consideration of this will be given in a later section.

From the  $23^\circ$  surface pressure coefficient plots, vortex breakdown is clear from a dramatic change in the pressure coefficient distribution. Figure 8 shows the behaviour of the axial velocity through the vortex core and the location of vortex breakdown is clear for each of the solutions. This is taken as the location where this velocity becomes zero. The locations for vortex breakdown for this case correspond to approximately  $x/c_r = 0.68$  for EADS,  $x/c_r = 0.67$  for NLR and  $x/c_r = 0.57$  for the Glasgow results. Upstream of the breakdown location, it is clear that there is some difference in the predicted maximum axial velocities, possibly caused by the differences in grid treatments between each of the solutions. It has also been found upstream of breakdown that the trajectory of the vortex system has moved inboard with the increase in incidence and that the strong primary and secondary vortices are still discernible. Inboard of the location of vortex breakdown a region of high pressure is found which corresponds to the location of a normal shock in the flow. This shock is similar to that described for the pre-breakdown case and will also be discussed in more detail in the following section.

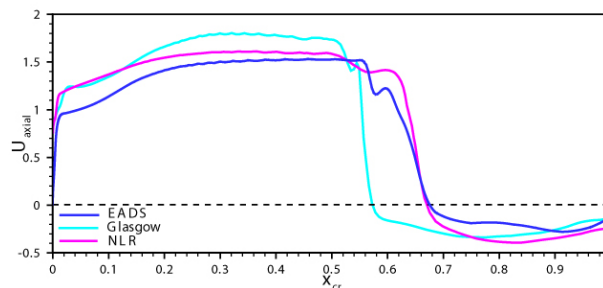


**Figure 8. Axial velocity through primary vortex cores for  $23^\circ$  post-breakdown case**

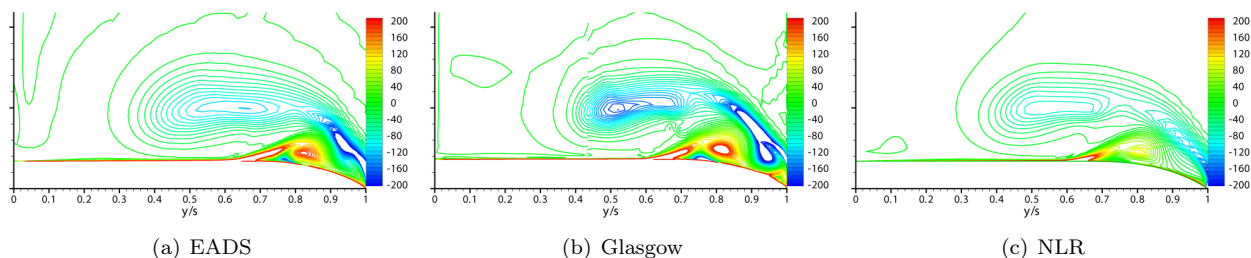


**Figure 9. Contours of  $x$  vorticity on a  $x/c_r = 0.4$  plane, for all results,  $\alpha = 23^\circ$ ,  $M = 0.85$ ,  $Re = 6 \times 10^6$**

A greater appreciation of the vortex core structure can be obtained by considering a slice through the vortex core at a constant streamwise location. Figure 9 shows the vortex core at a  $x/c_r = 0.4$  slice for each of the solutions for the post-breakdown case. Again, the relatively close agreement of the three solutions is clear. In each plot the elongation of the primary vortex is clear and the position of the vortex cores is almost identical. Both secondary and tertiary separation regions occur in the flow at this location for all solutions. However, as mentioned previously, the secondary vortex was slightly over-predicted in the Glasgow results and this can be clearly seen from these slices. Outboard of the secondary vortex, a thickening of the shear layer region is found in all three solutions, however the strength of this region appears to be directly linked to the relative strength of the secondary vortex. In the Glasgow results this region appears as a fourth vortex within the shear layer region with the same sign vorticity as the primary vortex. Therefore, it may be concluded that the thickening of the shear layer in this region is due to the secondary flow interacting with the shear layer which is closer to the wing surface due to the transonic conditions and the highly curved nature of the wing leading edge. With the increased strength of the Glasgow secondary vortex, this interaction results in a small vortical region. Downstream toward the trailing edge this vortical region dissipates and does not appear in the shear layer for any of the solutions, a fact which could also be attributed to an overall weakening of the secondary flow with streamwise location.

### C. CFD Sensitivity Study

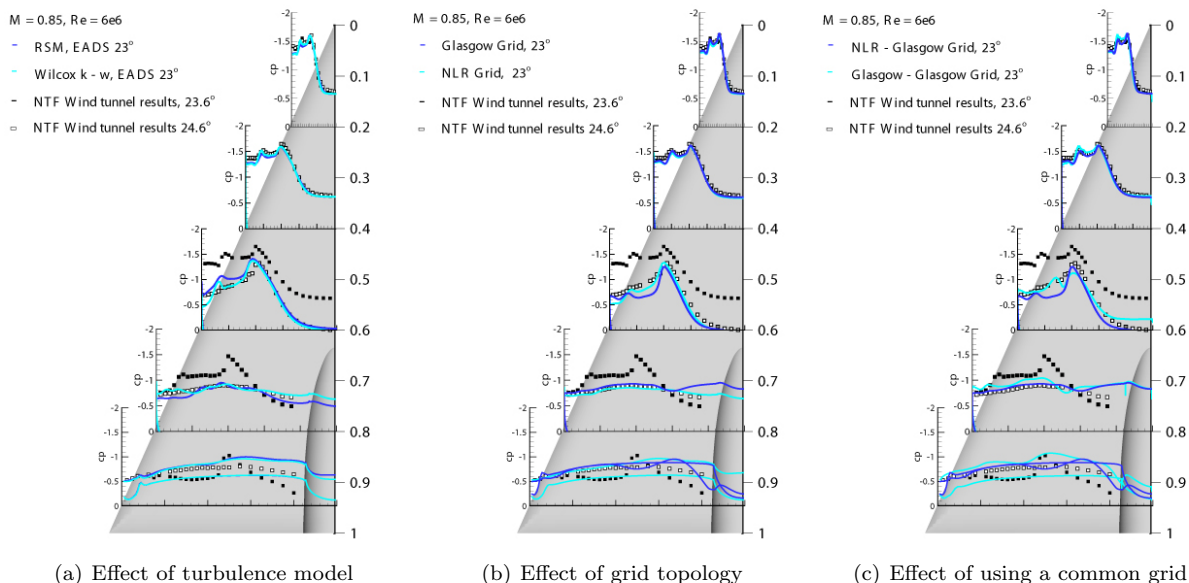


**Figure 10.** Effect of computational factors on flow solutions with comparison to Experiment for  $M = 0.85$ ,  $Re = 6 \times 10^6$  and  $\alpha = 23^\circ$ ; a) Comparison between RSM and Wilcox  $k-\omega$  model (EADS Results); b) Comparison between results from Glasgow and NLR grids (NLR Results); c) Comparison between Glasgow and NLR results on common grid using similar turbulence model.

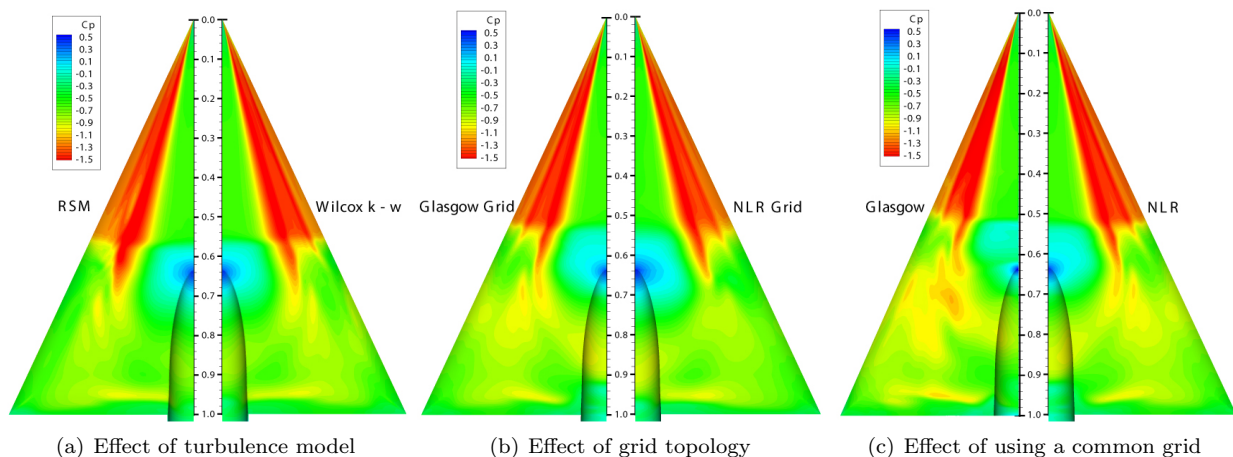


**Figure 11.** Contours of surface pressure coefficient showing effect of computational factors on flow solutions with comparison to experiment for  $M = 0.85$ ,  $Re = 6 \times 10^6$  and  $\alpha = 23^\circ$ ; a) Comparison between RSM and Wilcox  $k-\omega$  model (EADS Results); b) Comparison between results from Glasgow and NLR grids (NLR Results); c) Comparison between Glasgow and NLR results on common grid using similar turbulence models.

For the post-breakdown  $\alpha = 23^\circ$  case, consideration was given to the effect of a number of computational parameters, such as the turbulence model, grid topology and solver used, on the flow solutions. The results of these investigations are shown in Figures 10 and 11. To consider the effect of the turbulence model on the flow, a comparison between the two models used by EADS and the experimental data is shown in Figure 10(a). These models are the standard Wilcox  $k-\omega$  and the Reynolds Stress model which are implemented in the FLOWer code. Upstream of breakdown there is little effect of turbulence model on the predicted flow behaviour. Vortex breakdown is predicted to occur on the wing downstream of the  $x/c_r = 0.6$  location for both cases, with only a minor difference outboard in the secondary vortex location. This difference is due to vortex breakdown being predicted further downstream for the RSM model as determined from the normal shock location close to the symmetry plane in Figure 11(a). Downstream of breakdown, differences in the

pressure coefficient distributions are apparent, but the agreement with the  $24.6^\circ$  experimental data point is relatively good for both models. Overall, the differences are subtle and therefore, it may be concluded that the effect of turbulence model on the flow predicted is minimal for this case.

The effect of grid topology was also considered by running the same solver and turbulence model on two of the grids with differing topologies. These were the H-H grid of Glasgow and NLR's C-O grid. It is clear from Table 1 that the overall sizes of the grids are quite different. However, this is mostly due to the topology and chosen far-field definitions and it is found that the number of grid points over the wing surface is similar for both the normal and spanwise direction. For the streamwise direction the grids are not similar at all with the Glasgow grid having approximately twice the number of grid points than the NLR grid. However, keeping this difference in resolution in mind, it is felt that a comparison can be made. The results of this comparison are shown in Figures 10(b) and 11(b). The pressure coefficient distributions show very little difference between the solutions, both upstream and downstream of breakdown. However, when considering the pressure coefficient contours overall, as shown in Figure 11(b), it is clear that there are some notable differences in the flow, such as apparent strength of the normal shock and the suction peaks of the vortical system in the region of this shock. This is most likely to be caused by the difference in axial grid refinement mentioned above rather than the topology of the grids. Therefore, as with the turbulence model, it would appear that the topology of the grids has a very small influence on the predicted flow behaviour.

Both of these considerations can also be confirmed by making a comparison between the solutions for PMB and ENSOLV on a common grid. As shown in Table 1, the turbulence models used by these two institutions are similar, with the difference mainly in the specification of the turbulence model diffusion coefficients.<sup>26</sup> It is clear that the solutions are very similar, with only slight alterations of the flow behaviour downstream of breakdown. Looking at the surface pressure coefficient plot, for this case, the location of the normal shock and the breakdown behaviour of the flow is very similar. Thus, from these studies it has been shown that the type of grid and the choice of turbulence models has little impact on the predicted behaviour for these conditions. However, grid refinement particularly in the axial direction is important.

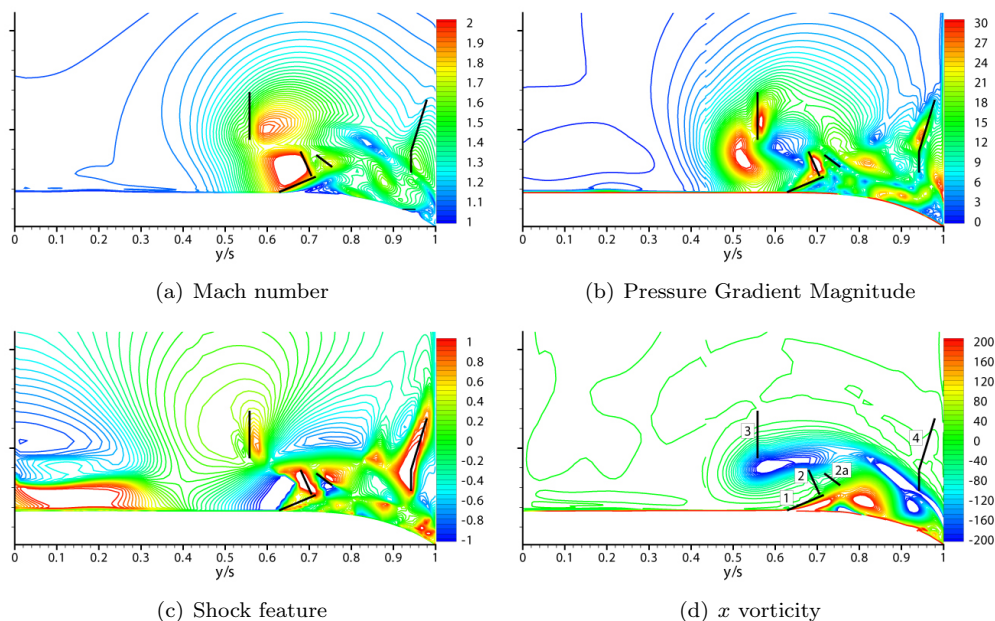


**Figure 12. Plots for  $x/c_r = 0.4$  showing contours of flow variables to highlight locations of cross flow shocks for  $\alpha = 18.5^\circ$  (Glasgow Results)**

## D. Shocks in the flow

### 1. Cross-flow Shocks

Evidence of a complex cross-flow shock system, beneath and around the primary and secondary vortices was found from consideration of the flow structure in a plane normal to the wing surface and the freestream direction using the methods described previously. An example of this flow behaviour from the Glasgow solution at  $x/c_r = 0.4$  for the pre-breakdown case is shown in Figure 12. Each of the proposed shock locations are marked on the variable contour plots. Outboard of the primary vortex suction peak there is a sharp change in pressure. This change is clear for both incidences from the surface pressure coefficient contours of Figure 6 and also from the computational and experimental distributions shown in Figure 5. Outboard of the secondary vortex peak another similar region exists in the computational and experimental results, particularly for the pre-breakdown flow for the  $\alpha = 23^\circ$  case. These sharp changes in  $C_p$  indicate the presence of cross-flow shocks as described in the introduction and shown in Figure 1.

The cross-flow shock found from the surface pressure coefficient contours is denoted by [1] on the diagram showing contours of  $x$  vorticity. This shock occurs in the flow for a constant non-dimensional spanwise location, defining a conical ray from the apex of the wing. These locations are approximately  $y/s = 0.64$  for all the  $\alpha = 18.5^\circ$  solutions and  $y/s = 0.62$  for the  $\alpha = 23^\circ$  solutions. With closer inspection, it was found that coinciding with the location of the shock close to the wing, the boundary layer thickens and separates to form the secondary vortex. Therefore, it may be suggested that this separation is due to an interaction between the shock and the boundary layer. Between this separation region and the primary vortex, the spanwise flow behaves in a similar manner to that in a convergent-divergent duct and accelerates to supersonic conditions. At some point, the flow can no longer maintain these high velocities and a shock appears to decelerate the flow. This is likely to be the cause of shocks [2] and [2a] in Figure 12. Shock [2a] appears to occur due to the flow accelerating again beyond shock [2]. It is not clear at this point whether shock [1] and shock [2] are connected or interact, however, it appears that they sit very close and it is possible that shock [2] is a stronger continuation of shock [1]. If this is indeed the case, the resulting shock curves upward from the surface to the primary vortex, as suggested by the diagram of Figure 1. From the literature, it is known that a shock sits in the region between the primary vortex and the surface of the wing.<sup>11,13</sup> However, there is little existing data which confirms the shape of this shock.

Two other shocks were found to occur in the cross-flow. Shock [3] is found to sit above the primary vortex and is similar to that found in the computations of Gordnier and Visbal<sup>16</sup> and Shock [4] sits above the primary shear layer, close to the leading edge. Both these shocks are likely to be caused by the curvature

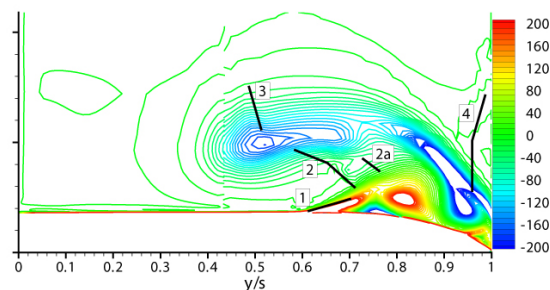
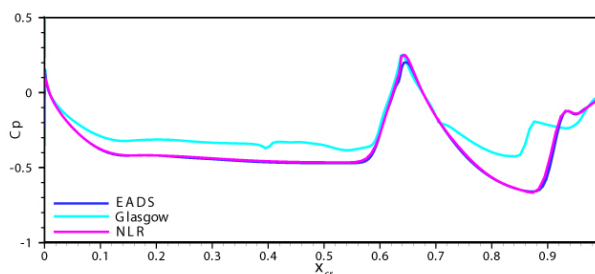
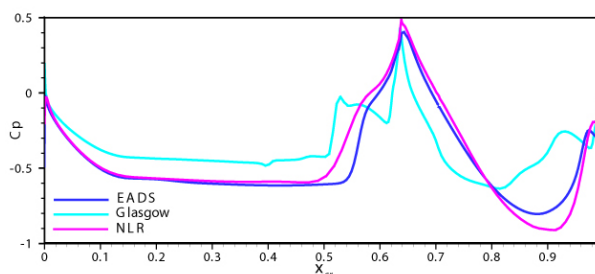


**Figure 13. Contours of  $x$  vorticity on a  $x/c_r = 0.4$  plane, highlighting locations of cross flow shocks for  $\alpha = 23^\circ$  case (Glasgow Results)**



(a)  $18.5^\circ$



(b)  $23^\circ$

**Figure 14. Pressure coefficient distribution at the symmetry plane on the wing**

of the shear layer causing the flow to accelerate up to conditions which cannot be sustained. All these shock were also found to occur for the  $\alpha = 23^\circ$  case, although the locations are different due to the inboard movement and relative increase in size of the vortical system. This is shown in Figure 13. It should be noted that the second sharp increase in pressure coefficient found outboard of the secondary vortex in the pressure coefficient distributions was not evident from the cross-flow planes.

## 2. Normal Shocks

Normal shocks are also found to occur in this flow, and are determined from plotting the pressure coefficient along the symmetry plane for each of the results as shown in Figure 14. From Figure 14(a), it is clear that despite slight differences between the results there are two normal shocks occurring at the symmetry plane. The first occurs upstream of the sting tip at approximately  $x/c_r = 0.6$ , which is most likely to be caused by the sting geometry. Further downstream at approximately  $x/c_r = 0.9$  in the EADS and NLR results and earlier at  $x/c_r = 0.85$  in the Glasgow results a second shock is found. This second shock is likely to correspond to the rear/terminating shock as described in the literature<sup>1,10,18</sup> for similar conditions. The difference in strength and location of these shocks is likely to be due to the nature of the grids. A third compression region is also found close to the trailing edge, and a third shock is found from the surface pressure contours at this location outboard of the symmetry plane on the wing surface. A shock occurring at this location is likely to be caused by the high curvature of the wing geometry and the necessity of the flow to return to freestream conditions at the trailing edge.

At an incidence of  $23^\circ$ , the behaviour at the symmetry plane shows the shock at the sting tip at approximately  $x/c_r = 0.6$ , but with a second shock occurring in the flow slightly upstream of this location. This is shown more clearly for the Glasgow results which show two clear, strong shocks than for the EADS and NLR results which show the compression of two shocks, which appear to merge into one. The difference in shock strength is likely to be caused by variations in grid refinement, particularly in the axial direction. This will cause the solutions to have varying shock resolutions, which was mentioned in the previous section. Despite the variation of shock strength, the locations of these shocks are similar with the upstream shock occurring at about  $x/c_r = 0.52$  for both the NLR and Glasgow results and slightly downstream at  $x/c_r = 0.56$  for the EADS results. It may be noted that for both incidences there are three normal shocks occurring on the wing. For an incidence of  $23^\circ$ , it is clear that the rear/terminating shock described for the  $\alpha = 18.5^\circ$  case is no longer evident and that a new second shock is apparent upstream of the sting tip. From the behaviour described in the investigations of Elsenaar and Hoeijmakers<sup>10</sup> under similar conditions, it is possible that this shock upstream of the sting tip is the rear/terminating shock having undergone an upstream shift with the increase of incidence. However, due to the presence of the sting and the shock caused by this geometry, it not possible to state this conclusively. Close to the trailing edge, as also found in the experiments, a second normal shock is observed, however this is likely to be the same trailing edge shock as found for  $\alpha = 18.5^\circ$ .

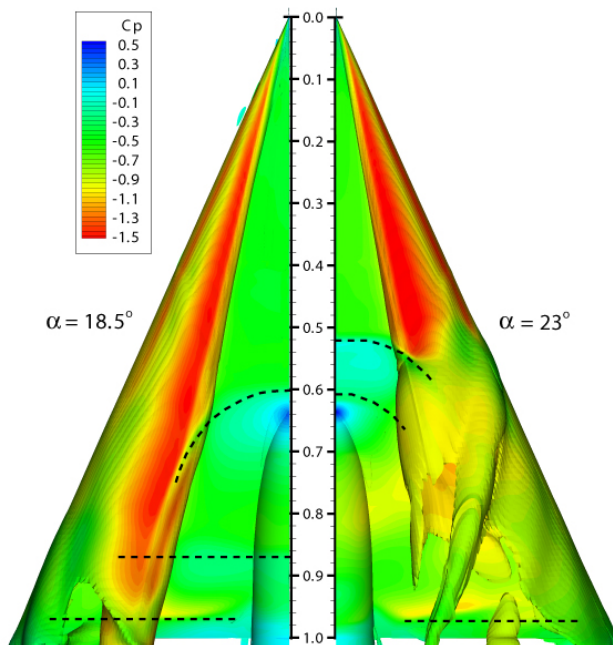


**Figure 15. Isosurface of  $x$  vorticity coloured by pressure coefficient showing primary vortex shear layer and normal shock shape (Glasgow Results)**

Considering the three-dimensional behaviour of the normal shocks, it is found that the shock occurring upstream of the sting tip curves downstream and intersects the rolled up shear layer of the vortex as shown in Figure 15 and highlighted by the dashed lines. This is in agreement with the observations of Donohoe and Bannink<sup>1</sup> and the schematic shown in Figure 1 for the rear/terminating shock. However, it is likely

that this curvature is caused by the sting presence for this configuration. Also highlighted are the locations of the other normal shocks found in the flow and described above. The rear/terminating shock in the  $18.5^\circ$  solution is found to be normal to the freestream and wing surface and does not appear to curve downstream outboard of the symmetry plane. This lack of curvature may be due to the influence of the sting on the flow, as previous investigations have considered a flat wing without sting support. Also clear from this plot are the two cross-flow shocks which sit above the vortex described above ([3] and [4] from Figures 12 and 13). It is possible, for both incidences, that there is an interaction between these cross-flow shocks and the normal sting tip shock, which will further increase the complexity of the flow in this region. However, further experimental data is needed in this region to determine this behaviour.

### E. Shock/Vortex Interaction and Vortex Breakdown

As mentioned, it appears that the sting tip shock intersects the vortex system and therefore it is highly likely that some form of shock/vortex interaction takes place, particularly for higher incidences. To consider this, the pressure and pressure gradient in the freestream direction through the vortex cores for both incidences were analysed. These are shown in Figure 16 using the Glasgow solutions, with the calculated pressure ratios for each proposed shock/vortex interaction location marked. For the  $\alpha = 18.5^\circ$  case, the interactions occur without vortex breakdown, and it has been previously suggested that this is due to the shock sitting above the vortex core.<sup>1</sup> However, from consideration of the vortex core properties it is found that there are three regions of adverse pressure gradient which may suggest direct interactions. These coincide with the two normal shocks at the symmetry plane and the trailing edge shock detailed previously. The pressure ratios for all three are less than 1.5 and, as shown, the primary vortex recovers after passing through each. Therefore, it may be suggested that these are weak interactions.

For the  $\alpha = 23^\circ$  case, where breakdown occurs on the wing, it is clear that there are two regions of high adverse pressure gradient at the vortex core. The first coincides with the location of the normal shock upstream of the sting tip as shown at the symmetry plane in Figure 14 and also with the onset of vortex breakdown. Very close to this, the second, higher, pressure gradient coincides with the occurrence of complete vortex breakdown, which can be seen in Figure 8. These pressure gradients have pressure ratios of 2.06 and 3 respectively. It is likely that the first pressure increase is due to the weak effect of the normal shock at the symmetry plane on the vortex core, in a similar manner to the interaction at the lower incidence. The second pressure gradient is much stronger and may indicate a direct interaction between the downstream section of the shock and the vortex core and indeed this location corresponds to the region where the shock intersects the vortex core as demonstrated for the Glasgow results in Figure

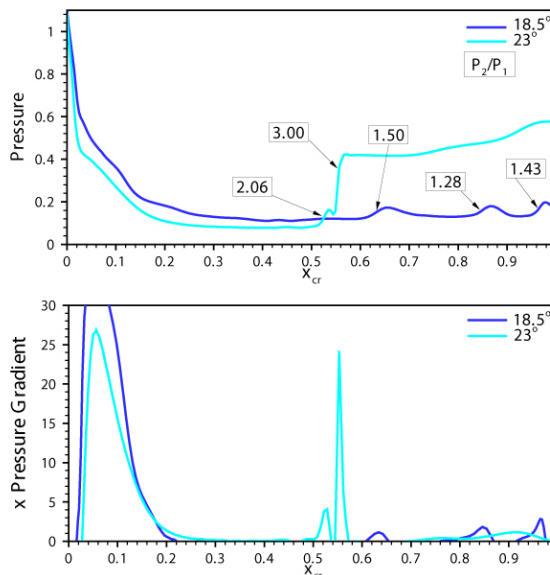


Figure 16. Pressure distribution through vortex cores with corresponding  $x$  pressure gradient for both incidences; The numbers on the plot in a) signify the magnitudes of the pressure ratios through the intersecting shocks. (Glasgow Results)

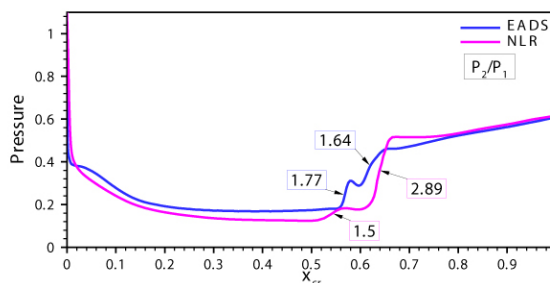


Figure 17. Pressure distribution through vortex cores for EADS and NLR solutions, similar to Figure 16

15. Considering the vortex core data for both EADS and NLR results, as shown in Figure 17, a similar behaviour is witnessed. However the predicted shock strengths at the point of breakdown are lower in the EADS and NLR solutions in comparison to the Glasgow results. The pressure ratios through the shocks for the  $\alpha = 23^\circ$  case are approximately 1.77 and 1.64 for the EADS solution and ratios of 1.5 and 2.89 for NLR. There may be a number of reasons for this difference in shock strength between each of the solutions, such as grid refinement, turbulence model and solver treatment. However, despite the differences in flow solutions and computational set-up, the locations and effect of the shocks on the flow are the same. These differences may also be due to the differences in predicted axial velocity through the vortex cores, as shown in Figure 8. The Glasgow solution has predicted a maximum axial velocity which is higher than for the EADS and NLR solutions. As a result of this increase in axial velocity the Mach number upstream of the shock will increase, and the upstream pressure will reduce, resulting in a stronger shock to maintain flow equilibrium. Thus, it is suggested that the difference in shock strength between the solutions, may also be caused by the upstream flow predictions.

It has been shown that there are interactions between the shocks and vortex core for both incidences, with weaker interaction occurring for the lower incidence. Due to this, it may be suggested that there is a limiting behaviour below which the vortex can retard the effects of the shock and remain coherent. Above this limit, the interaction causes a considerable weakening of the vortex core, which results in the vortex being unable to sustain itself and vortex breakdown to occur. Based on the differences in the flow solutions described above, it may be suggested that this limit is dependent on both the axial velocity and strength of the vortex and the relative strength of the shocks acting in the flow. The strength of the shock may also be dependent on the upstream axial flow. In his comprehensive review, Deléry<sup>5</sup> demonstrated the importance of a number of parameters for vortex breakdown caused by shock/vortex interaction. These include the tangential or swirl velocity,  $U_\theta$ , and the axial velocity of the vortex core,  $U_x$ . He also proposed that the swirl ratio or the Rossby number may be used as a measure of the vortex intensity and thus the susceptibility of the vortex to shock induced breakdown. It was also suggested that the strength of the shock necessary for breakdown was directly related to the vortex intensity, as the Rossby number is decreased, the strength of the shock needed for breakdown decreases. The Rossby number is a non-dimensional parameter, defined as the ratio of the axial and circumferential momentum in a vortex and is given by:

$$Ro = \frac{U_x}{r_c \Omega} = \frac{U_x}{U_\theta}$$

In this investigation, the Rossby number is calculated as the ratio of the maximum axial velocity at the vortex core to the maximum swirl velocity of the vortex and is the inverse of the axial swirl parameter described in Ref. 5 and used as a breakdown criterion for a free-vortex. The criterion for breakdown using the Rossby number has also been investigated by Spall *et al.*<sup>27</sup> and by Robinson *et al.*,<sup>28</sup> who applied it to computational results on delta wings and determined that the limiting Rossby number occurs between 0.9 and 1.4 for most cases, with a stable vortex core occurring for values above 1.4. As a vortex passes through a normal shock, the tangential velocity is found to stay relatively constant while the axial velocity decreases, thus reducing the Rossby number. With the reduction in the Rossby number comes an increase in vortex intensity and, as a result, the susceptibility of the vortex to breakdown increases. This susceptibility is also linked to the strength of the impinging shock and thus is also dependent on the upstream Mach number.<sup>29</sup> In a review by Kalkhoran and Smart<sup>29</sup> a vortex breakdown limit is discussed for vortices with uniform Mach number profiles, however little data exists to determine a limit for delta wing vortices which have jet-like

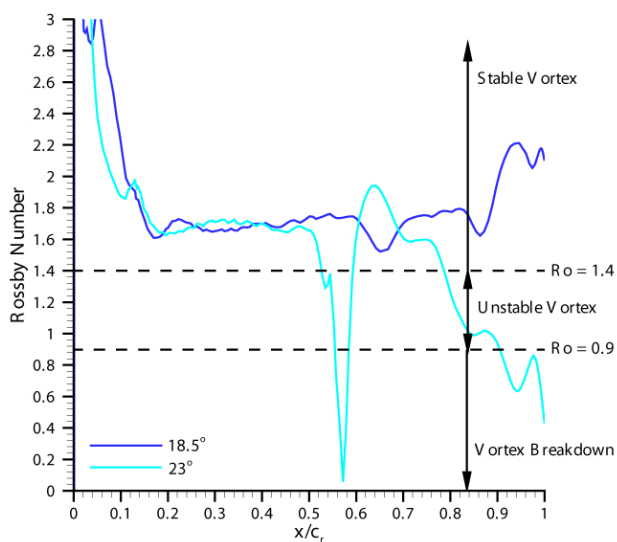


**Figure 18. Rossby number distribution against root chord location for pre- and post-breakdown cases (Glasgow Results)**

velocity profiles.

The Rossby number was calculated using the Glasgow solutions for both incidences and the resulting graph is shown in Figure 18 with respect to streamwise location on the wing. Also noted on the plot are the critical Rossby numbers for vortex breakdown. From these results it is clear that although there is a weak interaction between the vortex and normal shock at  $x/c_r = 0.62$  at an incidence of  $18.5^\circ$ , the Rossby number does not decrease significantly and does not cross the limit for breakdown. This means that the vortex is not sufficiently weakened by the shock and a recovery is witnessed downstream. Further downstream this occurs again, for the locations corresponding to where the rear and trailing edge shocks would intersect the vortex core, however the vortex is still strong enough to retard their influence. For the  $23^\circ$  case, a similar Rossby number profile is noted upstream of  $x/c_r = 0.45$  but downstream of this location, the behaviour is quite different. A similar behaviour is noted as for the pressure gradients in Figure 16 where it appears that at  $x/c_r = 0.51$  the vortex is affected by the normal shock, which weakens it and reduces the Rossby number as before. The reduction is greater than for the  $18.5^\circ$  incidence and results in a Rossby value which is within the unstable vortex region, however vortex breakdown does not occur at this stage, in fact again there is a slight recovery. Complete vortex breakdown is then caused by the vortex being intercepted by what appears to be a second shock at approximately  $x/c_r = 0.55$  which has a greater effect on the already weakened vortex flow, and breakdown is almost immediate. This location coincides with point at which the downstream curved section of normal shock intersects the vortex core region in Figure 15. Beyond the minimum Rossby number, which signifies the point at which the axial velocity becomes zero, the Rossby number appears to increase again, this is due to the recirculation of the breakdown flow and appears as a increase due to the magnitude of axial velocity being used in the calculation.

As mentioned above, the limit of the flow behaviour which causes breakdown to occur is also dependent on the strength of the shocks which appear in the flow and the upstream Mach number. The strength of a shock is usually determined by the size of the pressure ratio across the shock,  $P_2/P_1$  as described above and in Figure 16. Thus, if the shock is suitably strong and the vortex is susceptible to vortex breakdown then conditions are set for breakdown to occur. Although a critical value for the Rossby number has been suggested from previous investigation, there is no data for a critical shock strength. However, from the results of this investigation, it may be supposed that a limit exists. In this case the limit has been reached and the strength of the shock is high enough to cause a complete reorganisation of the flow behaviour of the already weakened vortex. The current results, as detailed, show that for a higher axial velocity a stronger shock is required for breakdown to occur. This is in agreement with the relation between the vortex intensity and shock strength for vortex flows with uniform axial flow distributions. However, further experimental data and theoretical reasoning is needed to determine if these results form a trend for all conditions.

## IV. Discussion

Having considered the mechanisms which cause vortex breakdown to occur on the wing, it is possible to return to the issue of the discrepancies between the CFD and experimental results. It was found from the experimental data used in this study that vortex breakdown jumps abruptly from a location downstream of the trailing edge to a location upstream on the wing for a small increases in incidence. In this case, the flow seems to go from full vortical flow over the whole wing surface to breakdown occurring close to the  $x/c_r = 0.6$  location in a one degree increase. As the occurrence of breakdown was being predicted early on the wing in the computational solutions, further calculations were performed at intermediate incidences to validate the behaviour of the onset of vortex breakdown. These results are shown in Figure 19 which contains the results for both EADS and Glasgow compared to experimental data. From this plot it is clear that the behaviour of the onset of vortex breakdown is very similar between the CFD and experiment, however the angle at which this occurs varies. The exact location of vortex breakdown is not known, however from the surface pressure coefficient distributions the approximate locations could be determined. With further consideration of the literature it was found that there is a large spread of values for this critical angle. These are detailed in Table 2 below. It is quite clear from all these results that the critical onset angles for vortex breakdown over the wings for current CFD solutions are much earlier than for the majority of the experimental results.

**Table 2. Critical Incidence for transonic vortex breakdown to be witnessed on 65° delta wings**

Source	Type	Conditions	$\alpha_{cr}$
Elsenaar and Hoeijmakers <sup>10</sup>	exp.	$M = 0.85, Re = 9 \times 10^6$	23°
Houtmann and Bannink <sup>18</sup>	exp.	$M = 0.85, Re = 3.6 \times 10^6$	20°
Chu and Luckring <sup>20</sup>	exp.	$M = 0.799, Re = 6 \times 10^6$	26.6°
"	exp.	$M = 0.831, Re = 6 \times 10^6$	24.6°
"	exp.	$M = 0.851, Re = 6 \times 10^6$	24.6°
"	exp.	$M = 0.871, Re = 6 \times 10^6$	24.7°
"	exp.	$M = 0.9, Re = 6 \times 10^6$	22.6°
"	exp.	$M = 0.849, Re = 11.6 \times 10^6$	24°
Longo <sup>11</sup>	CFD	$M = 0.8, Inviscid$	25°
Present Investigation - Glasgow	CFD	$M = 0.85, Re = 6 \times 10^6$	20°
Present Investigation - EADS	CFD	$M = 0.85, Re = 6 \times 10^6$	21°

To explain this early prediction, further consideration is needed to the discussion given above considering a critical limit for breakdown to occur dependent on the vortex core strength and the strength and locations of the shockwaves in the flow. As shown, with an increase in incidence the strength of the shocks in the flow increases, most likely as a response to the increased acceleration of the flow over the wing surface. Similarly, the axial velocity in the vortex core increases and it has been shown that there is a critical relationship between these quantities which results in breakdown for a critical incidence. To change the angle at which vortex breakdown occurs, it will be necessary to have a change in either one of these parameters, for example with an increase in vortex intensity and therefore a decrease in axial velocity or an increase in tangential velocity, the strength of the shock needed to cause breakdown will decrease and breakdown will occur earlier on the wing.

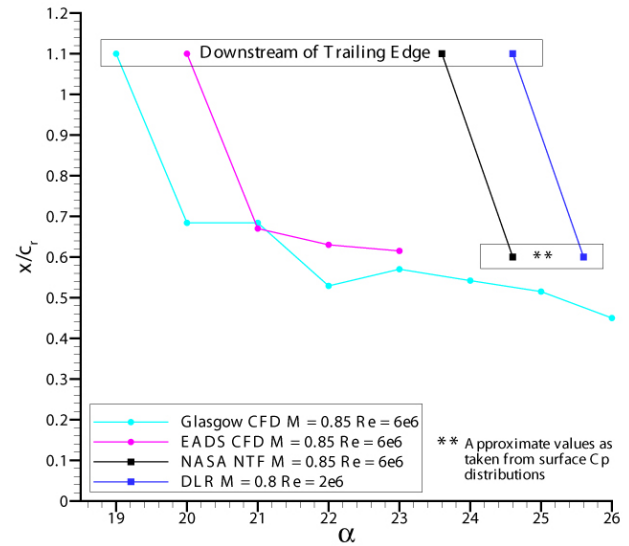


**Figure 19. Vortex breakdown location for both computational and experimental results**

Despite continuing improvement in CFD codes, turbulence models and practices, one region of vortical flows which has proved difficult to predict accurately is the axial flow through the vortex core. There have been a number of collaborations and investigations which have considered the vortical flows over delta wings and have generally predicted the flow behaviour well, however the axial velocity is almost always much lower than that found from experiments. This is due to both turbulence modelling and restrictions in grid refinement. To fully resolve the vortex core behaviour it would be necessary to have similar refinement as is applied to boundary layer regions. Due to this, and despite not having such data from the experiments, it may be assumed that the axial velocities predicted in the computational solutions of this investigation are much lower than those of the experiment. From the cross-sectional pressure coefficient distributions, it is clear that the strength of the shocks predicted are comparable to the experiment. This being the case, then vortex breakdown would occur much earlier for the same conditions.

## V. Conclusions

For all cases studied in this investigation, it was shown that there was good agreement between the computational solutions and the available experimental data. This shows that CFD can be used to predict the flow behaviour for transonic conditions. A thorough sensitivity study was carried out to determine the effect of a number of computational factors on the flow behaviour. A number of transonic flow features were determined from analysis of the solutions, particularly the occurrence of a complex cross-flow shock system and the abrupt behaviour of vortex breakdown. However, more experimental data, particularly considering the off-surface flow behaviour, is needed to both confirm the existence of these shocks and to further validate the flow solutions.

The mechanisms which determine the behaviour of transonic vortex breakdown were shown to be highly complex and are dependent on the vortex core strength and the strength and location of the shocks in the flow. Through consideration of computational flow solutions, a means to analyse the influence of each of these parameters has been established and it has been shown that a relationship must exist which has a critical limit for vortex breakdown to occur. Further research is needed, both experimental and computational, to confirm the behaviour of this relationship and to allow for further analysis of the critical limit of shock/vortex interactions for delta wing flows.

As stated in the introduction to this paper, this work was undertaken as part of the VFE-2, one of the facets of the RTO AVT-113 Task Group on “Understanding and Modelling Vortical Flows to Improve the Technical Readiness Level for Military Aircraft”. This task group has provided an excellent environment for research with both experimental and computational researchers able to collaborate closely on a common configuration. This encourages a situation where expertise can be shared which facilitates the research undertaken.

## Appendix

### A. Code Descriptions

#### 1. EADS-MAS - FLOWer 116.17

At EADS, the FLOWer Code version 116.17 was used, which was originally developed in a national German co-operative programme under the direction of DLR.<sup>30</sup> FLOWer solves the 3D, compressible, RANS equations in integral form in the subsonic, transonic and supersonic flow regimes. Turbulence is modelled by either algebraic or transport equation models. The numerical procedure is based on structured meshes and the spatial discretization uses a central cell-vertex, cell-centred or AUSM finite volume formulation with explicitly added dissipative terms. On smooth meshes, the scheme is second order accurate in time. The time integration is carried out by an explicit hybrid multistage Runge-Kutta scheme, which is accelerated by local time stepping and implicit residual smoothing. This solution procedure is embedded into a sophisticated multi-grid algorithm which allows a successive grid refinement with the option of simple or full multi-grid. FLOWer offers a flexible multi-block structure, enabling the treatment of complex aerodynamic configurations and can also be operated in a parallel mode.

For the present calculations the code was operated in a Jameson-type mode as a cell-centred, explicit, multi-grid scheme using a five-stage Runge-Kutta scheme for the time integration. The numerical dissipation model was the anisotropic dissipation model suggested by Martinelli and Jameson.<sup>31</sup> Additionally, the dissipative flux vector was optimised by a relaxation between old and new values within the Runge-Kutta scheme.

The standard Wilcox  $k-\omega$  turbulence model and a Reynolds Stress Model (RSM) are used to obtain the results presented here. The governing flow equations and the turbulence transport equations are solved synchronously within the time integration. Additionally the code is run in time accurate mode using the dual time stepping scheme with a large physical time step. This option very often overcomes convergence problems, as by the use of the dual time stepping scheme the solution develops synchronously. The solution at each physical time step is obtained rapidly through local time stepping, implicit residual smoothing and the use of a multi-grid strategy (3 level W-cycle).

## 2. Glasgow University - PMB

The PMB (Parallel Multi-Block) code is a multi-block structured solver which solves the unsteady RANS equations in a 3D Cartesian frame of reference.<sup>32</sup> The governing equations are discretized using a cell-centred finite volume approach combined with an implicit dual-time method. In this manner, the solution marches in pseudo-time for each real time-step to achieve fast convergence. Two methods are available for the discretisation of the convective terms, either Osher's upwind scheme<sup>33</sup> or Roe's flux-splitting scheme.<sup>34</sup> A MUSCL interpolation method is used to provide nominally third order accuracy and the van Albada limiter is also applied to remove any spurious oscillations across shock waves. The central differencing spatial discretisation method is used to solve the viscous terms, with the resulting non-linear system of equations generated being solved by integration in pseudo-time using a first-order backward difference. A Generalised Conjugate Gradient method is then used in conjunction with a Block Incomplete Lower-Upper (BILU) factorisation as a pre-conditioner to solve the linear system of equations, which is obtained from a linearisation in pseudo-time.

A number of one and two equation turbulence models are available to use in the solver, as well as the option of Large Eddy Simulation (LES) and Detached Eddy Simulation (DES). All the calculations carried out for this study use the Wilcox  $k-\omega$  turbulence model with a correction for vortical flows. It is well known that the standard model, as with most other two-equation models, over predicts the eddy viscosity within the vortex core which leads to exaggerated diffusion of vorticity. The enhanced model which was proposed by Brandsma *et al.*<sup>35</sup> controls the production of turbulent kinetic energy and hence eddy viscosity through an increase in the production of dissipation ( $\omega$ ) within regions of highly rotational flow. A suitable sensor has been used to distinguish between shear layers and vortex cores. Investigations carried out using this model for both subsonic<sup>36</sup> and transonic<sup>35,37</sup> conditions have found that the model performed well against experimental results.

All calculations performed were steady state, running for 4000 time steps and used an implicit CFL number of 5.0. Each computational run took approximately 24 wall clock hours running on 24 processors of the 128-processor/workstation Pentium 4 Beowulf cluster of the CFD Laboratory at the University of Glasgow.

## 3. NLR - ENSOLV

The flow solver ENSOLV,<sup>38-40</sup> which is part of NLR's CFD system ENFLOW, is capable of solving the Euler and Navier-Stokes equations on multi-block structured grids for arbitrary configurations. These configurations can be either fixed or moving relative to an inertial reference frame, and can be either rigid or flexible. Several turbulence models are available to use in the flow solver, including the TNT  $k-\omega$  model, the EARSIM model and a hybrid RANS-LES method, named eXtra-Large Eddy Simulation (X-LES). For all simulations in the present study, the TNT  $k-\omega$  model, which is a variant of the Wilcox  $k-\omega$  model, is employed with the same vortical correction as described for the Glasgow results. This TNT  $k-\omega$  model is better suited to the computation of vortical flows<sup>35</sup> and resolves the free-stream dependency of the solutions.<sup>26</sup> The equations are discretized in space by a cell-centred, finite-volume method, using multi-block structured grids, central differences, and matrix artificial diffusion. The artificial diffusion consists of a blending of second and fourth-order differences with a Jameson-type shock sensor for the basic flow equations and a TVD discontinuity sensor for the  $k-\omega$  equations.

For steady flow simulations, the discretized time-dependent system of equations is integrated toward the steady-state using a five-stage explicit Runge-Kutta scheme. Local-time stepping, implicit residual averaging and multi-grid acceleration techniques are applied. The source terms in the  $k-\omega$  equations are treated explicitly, while a separate time-step is used for the  $k-\omega$  equations to enhance the efficiency of the scheme. For time-accurate simulation, the flow solver uses the dual-time stepping scheme, where for each time-step the time-dependent flow equations are integrated in pseudo-time toward a steady-state in a similar way as in the steady flow simulation using the same acceleration techniques.

All simulations performed were steady state. During all simulations, grid sequencing has been used, with 1500 iterations on all four grid levels. Each simulation took approximately 8 wall clock hours running on 2 processors of NLR's NEC SX5/8B.

## B. Grid Descriptions

### 1. EADS-MAS

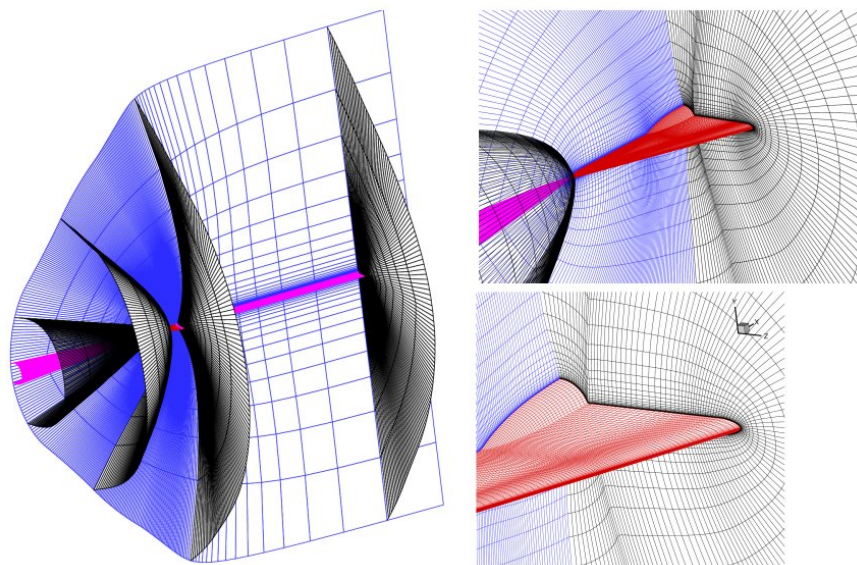


Figure 20. 3D Details of the EADS grid

The EADS computational grid is a conical C-O grid, which has a singular line from the apex of the wing toward the upstream far field boundary. In the plane of symmetry, the grid wraps as a C-Mesh around the apex of the wing and for constant spanwise locations an O-Type topology is applied. Using a conical grid allows for a very fine resolution of the apex of the wing. Behind the wing, the O-mesh orientation of the last wing section is kept toward the far field boundary. The grid has been generated using a 3-D hyperbolic grid generator. The hyperbolic partial differential equations specify orthogonality and volume control. To avoid intersections of the grid lines in concave corners (for example, the sting fairing) numerical dissipation is added to the equations. The sting is included in the surface definition of the wing. This means that the wing-sting intersection is not always mapped as an exact line in the grid. From the wing trailing edge, the sting is kept as a cylindrical body with constant cross section down to the far field boundary. Figure 20 gives an overall view of the 3-D grid structure.

The grid used has an overall size of approximately  $10.6 \times 10^6$  grid points, which corresponds to a distribution of 321 grid points in the streamwise direction, 129 grid points spanwise and 129 grid points normal to the surface of the wing. The grid, as all grids used in this investigation, only considers a semi-span wing. It has been generated as a single block grid (one simply connected topological region). However, for use in parallel mode, the grid has been subdivided into 24 more or less equally sized blocks.

### 2. Glasgow University

The structured multi-block grid of the University of Glasgow was created using the Icemcfd mesh generation package, Hexa. The semi-span geometry was exactly reproduced to approximately one chord length downstream of the trailing edge, at which point an approximation to the experimental sting (See Figure 4) was made to the far field. This accuracy of the sting was chosen based on the recommendations of Allan *et al.*,<sup>41</sup> who found that the effect of a sting or support apparatus was negligible downstream of a distance one root chord from the trailing edge. The domain was relatively large in size with the far field being defined  $20c_r$  in each direction from the wing apex to minimise the effect of the boundaries on the flow. A H-H topology was chosen for the wing with a collapsed edge at the apex of the wing. Convergence problems associated with this singularity were dealt with by using laminar flow at the apex and fixing transition to turbulence at a constant streamwise location ( $x = 0.4$ ) in the grid. This location was initially considered based on the investigation carried out by Morton<sup>42</sup> for a subsonic  $70^\circ$  delta wing flow. From a short study, it was found that the transonic flow solution is relatively insensitive to the location of the fixed transition and so it was

felt that the  $x = 0.4$  location was satisfactory.

As this case involved a wing-sting arrangement, a slightly different approach to structured grid generation was needed than that for a wing alone case. In order to allow for a smooth grid point distribution and refinement of the grid in this area, a structured Ogrid was used around the sting. An example of this is shown in Figure 21. Overall, the blocking structure was optimised for cell geometry and therefore, reduced skewness, particularly in the sting tip region and as a result a total of 353 blocks were used. The overall size of the grid was approximately  $7 \times 10^6$  grid points, with a distribution across the blocks which allowed for an efficient load balance of grid points across the 24 processors used for the calculation. The distribution of the grid points across the wing, translate to 228 streamwise, 170 spanwise and 81 normal to the wing (in the first block above the wing surface, which contains the region of interest). The first wall spacing used was  $1 \times 10^{-5}c_r$  which gave a  $y^+$  value of 2.2 over the wing surface and there are approximately 20 grid points in the boundary layer region.

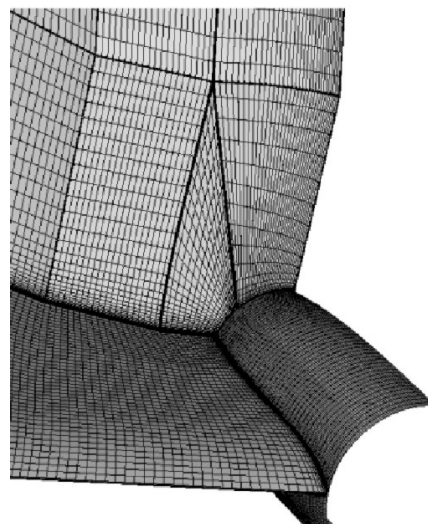
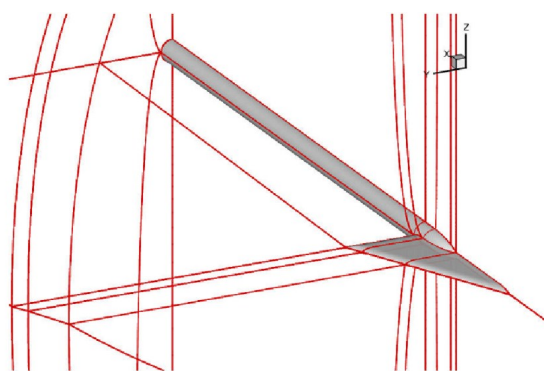


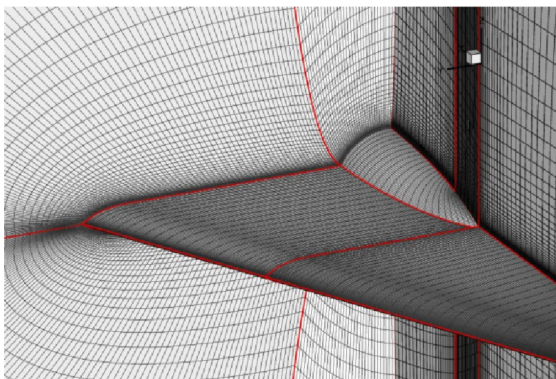
Figure 21. Ogrid topology around sting region

### 3. NLR

The NLR multi-block structured grid was generated using NLR's in-house grid generation tools present in NLR's CFD system ENFLOW.<sup>40,43</sup> A C-O-topology was chosen with a singular line emanating from the apex to the upstream far-field boundary. Details of the grid are shown in Figure 22. The far-field boundaries were approximately located at two reference wing chords before the model, three reference wing chords behind the model, three reference wing chords above and below the model and 2.4 reference wing chords beside the model. The grid consists of 12 blocks and approximately  $4.1 \times 10^6$  grid points, which allowed computation on four multi-grid levels. The distribution of the grid points translate to 112 grid points in the stream wise direction across the wing, 192 grid points in the span wise direction around the wing and 96 grid points normal to the wing. The spacing of the first grid cell normal to the surface was set to  $2 \times 10^{-6}c_r$ , which resulted in a  $y^+$  of approximately one. Away from the wall, the spacing increases by a ratio of approximately 1.1. Grid smoothing has been used to improve the quality of the grid. All calculations performed were fully turbulent.



(a) C-O-topology around the VFE-2 delta wing



(b) Grid detail for Surface, symmetry plane and a plane normal to the flow direction

Figure 22. Details of the NLR grid

## Acknowledgments

The authors would like to thank all the members of the RTO Task Group AVT-113 and particularly Professor Hummel for their interesting and fruitful discussions during the production of this work.

## References

- <sup>1</sup>Donohoe, S. R. and Bannink, W. J., "Surface Reflective Visualisations of Shock-wave/Vortex Interactions Above a Delta Wing," *AIAA Journal*, Vol. 35, No. 10, 1997, pp. 1568–1573.
- <sup>2</sup>Escudier, M., "Vortex Breakdown: Observations and Explanations," *Progress in Aerospace Sciences*, Vol. 25, 1988, pp. 189–229.
- <sup>3</sup>Hoeijmakers, H. W. M., "Modelling and Numerical Simulation of Vortex Flow in Aerodynamics," *AGARD Conference Proceedings "Vortex Flow Aerodynamics"*, AGARD-CP-494, July 1991, pp. 1.1–1.46.
- <sup>4</sup>Deléry, J. M., "Physics of Vortical Flows," *Journal of Aircraft*, Vol. 29, No. 5, 1992, pp. 856–876.
- <sup>5</sup>Deléry, J. M., "Aspects of Vortex Breakdown," *Progress in Aerospace Sciences*, Vol. 30, No. 1, 1994, pp. 1–59.
- <sup>6</sup>Gursul, I., "Recent Developments in Delta Wing Aerodynamics," *Aeronautical Journal*, 2004, pp. 437–452.
- <sup>7</sup>Elsenaar, A., Hjemberg, L., Bütefisch, K. A., and Bannink, W. J., "The International Vortex Flow Experiment," *Validation of Computational Fluid Dynamics - AGARD-CP-437 Volume 1*, AGARD, 1988, pp. 9.1–9.23.
- <sup>8</sup>Hummel, D. and Redeker, G., "A New Vortex Flow Experiment for Computer Code Validation," *Proceedings of the RTO-AVT Symposium on "Advanced Flow Management: Part A - Vortex Flows and High Angle of Attack for Military Vehicles" - RTO-MP-069(I)*, NATO RTO, 2001, pp. 8.1–8.32.
- <sup>9</sup>Erickson, G., Schreiner, J., and Rogers, L., "Multiple Vortex and Shock Interactions at Subsonic, Transonic and Supersonic Speeds," AIAA-90-3023, 1990.
- <sup>10</sup>Elsenaar, A. and Hoeijmakers, H. W. M., "An Experimental Study of the Flow over a Sharp-Edged Delta Wing at Subsonic and Transonic Speeds," *AGARD Conference Proceedings "Vortex Flow Aerodynamics"*, AGARD-CP-494, July 1991, pp. 15.1–15.19.
- <sup>11</sup>Longo, J. M. A., "Compressible Inviscid Vortex Flow of a Sharp Edge Delta Wing," *AIAA Journal*, Vol. 33, No. 4, 1995, pp. 680–687.
- <sup>12</sup>Erickson, G. E. and Rogers, L. W., "Experimental Study of the Vortex Flow Behaviour on a Generic Fighter Wing at Subsonic and Transonic Speeds," *19th AIAA Fluid Dynamics, Plasma Dynamics and Lasers Conference*, AIAA-87-1262, June 1987.
- <sup>13</sup>Donohoe, S. R., Houtman, E. M., and Bannink, W. J., "Surface Reflective Visualization System Study to Vortical Flow over Delta Wings," *Journal of Aircraft*, Vol. 32, No. 6, 1995, pp. 1359–1366.
- <sup>14</sup>Kandil, O. A., Kandil, H. A., and Liu, C. H., "Shock-Vortex Interaction over a 65-degree Delta Wing in Transonic Flow," *AIAA 24th Fluid Dynamics Conference*, AIAA-93-2973, July 1993.
- <sup>15</sup>Kandil, O. A., Kandil, H. A., and Liu, C. H., "Supersonic Vortex Breakdown over a Delta Wing in Transonic flow," *AIAA 11th Applied Aerodynamics Conference*, AIAA-93-3472-CP, August 1993.
- <sup>16</sup>Visbal, M. R. and Gordnier, R. E., "Compressibility Effects on Vortex Breakdown Onset Above a 75-Degree Sweep Delta Wing," *Journal of Aircraft*, Vol. 32, No. 5, 1995, pp. 936–942.
- <sup>17</sup>Jobe, C. E., "Vortex Breakdown Location over 65° Delta Wings: Empiricism and Experiment," *Aeronautical Journal*, Vol. 108, No. 1087, 2004, pp. 475–482.
- <sup>18</sup>Houtman, E. M. and Bannink, B. J., "Experimental and Numerical Investigation of the Vortex Flow over a Delta Wing at Transonic Speeds," *AGARD Conference Proceedings "Vortex Flow Aerodynamics"*, AGARD-CP-494, July 1991, pp. 5.1–5.11.
- <sup>19</sup>Thomer, O., Schröder, W., and Krause, E., "Normal Shock Vortex Interaction," *Proceedings of the RTO-AVT Symposium on "Advanced Flow Management: Part A - Vortex Flows and High Angle of Attack for Military Vehicles" - RTO-MP-069(I)*, NATO RTO, 2001, pp. 18.1–8.10.
- <sup>20</sup>Chu, J. and Luckring, J. M., "Experimental Surface Pressure Data obtained on a 65° Delta wing across Reynolds number and Mach Number ranges: Volume 1 - Sharp Leading Edge," NASA Technical Memorandum 4645, NASA Langley Research Centre, Feb. 1996.
- <sup>21</sup>Chu, J. and Luckring, J. M., "Experimental Surface Pressure Data obtained on a 65° Delta wing across Reynolds number and Mach Number ranges: Volume 2 - Small Radius Leading Edge," NASA Technical Memorandum 4645, NASA Langley Research Centre, February 1996.
- <sup>22</sup>Chu, J. and Luckring, J. M., "Experimental Surface Pressure Data obtained on a 65° Delta wing across Reynolds number and Mach Number ranges: Volume 3 - Medium Radius Leading Edge," NASA Technical Memorandum 4645, NASA Langley Research Centre, February 1996.
- <sup>23</sup>Chu, J. and Luckring, J. M., "Experimental Surface Pressure Data obtained on a 65° Delta wing across Reynolds number and Mach Number ranges: Volume 4 - Large Radius Leading Edge," NASA Technical Memorandum 4645, NASA Langley Research Centre, February 1996.
- <sup>24</sup>Soemarwoto, B. I., Boelens, O. J., Allan, M., Arthur, M. T., Butefisch, K., Ceresola, N., and Fritz, W., "Towards the simulation of Unsteady manoeuvre dominated by vortical flow," *21st AIAA Applied Aerodynamics Conference*, AIAA Paper 2003-3528, June 2003.
- <sup>25</sup>Lovely, D. and Haimes, R., "Shock Detection from Computational Fluid Dynamics Results," AIAA Paper 99-3285, 1999.
- <sup>26</sup>Kok, J. C., "Resolving the dependence on freestream values for the  $k - \omega$  turbulence model," *AIAA Journal*, Vol. 38, No. 7, pp. 1292.

- <sup>27</sup>Spall, R. E., Gatski, T. B., and Grosch, C. E., "A Criterion for Vortex Breakdown," *Physics of Fluids*, Vol. 30, No. 11, November 1987, pp. 3434–3440.
- <sup>28</sup>Robinson, B. A., Barnett, R. M., and Agrawal, S., "Simple Numerical Criterion for Vortex Breakdown," *AIAA Journal*, Vol. 32, No. 1, January 1994, pp. 116–122.
- <sup>29</sup>Kalkhoran, I. M. and Smart, M. K., "Aspects of Shock Wave-Induced Vortex Breakdown," *Progress in Aerospace Sciences*, Vol. 36, 2000, pp. 63–95.
- <sup>30</sup>"FLOWer, Installation and User Handbook," DLR doc. Nr. MEGAFLOW-1001, DLR, Germany.
- <sup>31</sup>Martineli, L. and Jameson, A., "Validation of a Multigrid Method for the Reynolds Averaged Navier-Stokes Equations," AIAA Paper 88-0414, 1988.
- <sup>32</sup>Badcock, K. J., Richards, B. E., and Woodgate, M. A., "Elements of Computational Fluid Dynamics on Block Structured Grids using Implicit Solvers," *Progress in Aerospace Sciences*, Vol. 36, 2000, pp. 351–392.
- <sup>33</sup>Roe, P. L., "Approximate Riemann Solvers, Parameter Vectors and Difference Schemes," *Journal of Computational Physics*, Vol. 43, 1981, pp. 357–372.
- <sup>34</sup>Osher, S. and Solomon, F., "Upwind Difference Schemes for Conservation Laws," *Mathematics of Computing*, Vol. 38, 1982, pp. 339–374.
- <sup>35</sup>Brandsma, F. J., Kok, J. C., Dol, H. S., and Elsenaar, A., "Leading Edge Vortex Flow Computations and Comparison with DNW-HST Wind Tunnel Data," *Proceedings of the RTO-AVT Symposium on "Advanced Flow Management: Part A - Vortex Flows and High Angle of Attack for Military Vehicles" - RTO-MP-069(1) Loen, Norway*, NATO RTO, 2001.
- <sup>36</sup>Allan, M., *A CFD Investigation of Wind Tunnel Interference on Delta Wing Aerodynamics*, Ph.D. thesis, CFD Laboratory, Department of Aerospace Engineering, University of Glasgow, October 2002.
- <sup>37</sup>Dol, H. S., Kok, J. C., and Oskam, B., "Turbulence Modelling for Leading Edge Vortex Flows," *40th Aerospace Sciences Meeting and Exhibit*, AIAA Paper 2002-0843, January 2002.
- <sup>38</sup>Kok, J. C., "Mathematical Physical Model of ENSOLV Version 3.20; A Flow Solver for 3D Euler/Navier-Stokes Equations in Arbitrary Multi-block Domains," NLR-CR-2000-621, Nationaal Lucht- en Ruimtevaartlaboratorium, NLR, 2000.
- <sup>39</sup>Kok, J. C., "Mathematical Physical Model of ENSOLV Version 3.20; A Flow Solver for 3D Euler/Navier-Stokes Equations in Arbitrary Multi-block Domains," NLR-CR-2000-620, Nationaal Lucht- en Ruimtevaartlaboratorium, NLR, 2000.
- <sup>40</sup>Kok, J. C. and Prananta, B. B., "User guide of ENSOLV Version 5.01. A Flow Solver for 3D Euler/Navier-Stokes Equations in Arbitrary Multi-block Domains with Aeroelastic Capabilities," Tech. rep.
- <sup>41</sup>Allan, M. R., Badcock, K. J., Barakos, G. N., and Richards, B. E., "Wind-Tunnel interference effects on a 70° delta wing," *The Aeronautical Journal*, October 2004, pp. 505–513.
- <sup>42</sup>Morton, S. A., "High Reynolds Number DES Simulations of Vortex Breakdown over a 70° delta wing," *21st Applied Aerodynamics Conference*, AIAA Paper 2003-4217, June 2003.
- <sup>43</sup>Spekreijse, S. P. and Nijhuis, G. H., "User guide of Engrid version 4.20. A graphical interactive grid generator for arbitrary multi-block domains," NLR-CR-98436, Nationaal Lucht- en Ruimtevaartlaboratorium, NLR, 1998.